

Ligand-Induced Conformational Changes in the Crystal Structures of *Pneumocystis carinii* Dihydrofolate Reductase Complexes with Folate and NADP⁺ †,‡

Vivian Cody,^{*,§} Nikolai Galitsky,[§] Dawn Rak,[§] Joseph R. Luft,[§] Walter Pangborn,[§] and Sherry F. Queener^{||}

Hauptman-Woodward Medical Research Institute, Inc., 73 High Street, Buffalo, New York 14203, and Department of Pharmacology and Toxicology, Indiana University School of Medicine, Indianapolis, Indiana 46202

Received November 17, 1998; Revised Manuscript Received February 1, 1999

ABSTRACT: Structural data from two independent crystal forms ($P2_12_12_1$ and $P2_1$) of the folate (FA) binary complex and from the ternary complex with the oxidized coenzyme, NADP⁺, and recombinant *Pneumocystis carinii* dihydrofolate reductase (pcDHFR) refined to an average of 2.15 Å resolution, show the first evidence of ligand-induced conformational changes in the structure of pcDHFR. These data are also compared with the crystal structure of the ternary complex of methotrexate (MTX) with NADPH and pcDHFR in the monoclinic lattice with data to 2.5 Å resolution. Comparison of the data for the FA binary complex of pcDHFR with those for the ternary structures reveals significant differences, with a >7 Å movement of the loop region near residue 23 that results in a new “flap-open” position for the binary complex, and a “closed” position in the ternary complexes, similar to that reported for *Escherichia coli* (ec) DHFR complexes. In the orthorhombic lattice for the binary FA pcDHFR complex, there is also an unwinding of a short helical region near residue 47 that places hydrophobic residues Phe-46 and Phe-49 toward the outer surface, a conformation that is stabilized by intermolecular packing contacts. The pyrophosphate moiety of NADP⁺ in the ternary folate pcDHFR complexes shows significant differences in conformation compared with that observed in the MTX–NADPH–pcDHFR ternary complex. Additionally, comparison of the conformations among these four pcDHFR structures reveals evidence for subdomain movement that correlates with cofactor binding states. The larger binding site access in the new “flap-open” loop 23 conformation of the binary FA complex is consistent with the rapid release of cofactor from the product complex during catalysis as well as the more rapid release of substrate product from the binary complex as a result of the weaker contacts of the closed loop 23 conformation, compared to ecDHFR.

Pneumocystis carinii (pc)¹ is an opportunistic fungal pathogen that is responsible for significant mortality among immunocompromised patients such as those with AIDS (1, 2). Although current treatment has been with antifolate inhibitors of dihydrofolate reductase (DHFR), antifolates such as trimethoprim have only moderate selectivity for the inhibition of pcDHFR (3). Thus, there is still a need to design compounds with greater selectivity and affinity for pcDHFR compared to those of the human enzyme.

Transient-state kinetic data for pcDHFR reveal that there is a rapid hydride transfer to the folate substrate and a rapid dissociation of NADP⁺ from the product complex, and after NADPH binding, rapid dissociation of tetrahydrofolate (4). These data indicate a single, preferred pathway for catalysis,

in contrast to the multiple component pathways indicated for either human or bacterial DHFR. These results further suggest that in some aspects, the kinetics of pcDHFR more closely resemble those of the human (h) DHFR than of the bacterial enzyme. For example, the k_{cat} for folate binding to pcDHFR is more than 26 times that of ecDHFR, but is only 12 times that of hDHFR. However, the K_m for folate pcDHFR is 54 times that of hDHFR, but only 12.5 times that of ecDHFR (4, 5). Another feature important to catalysis is the overall charge of DHFR at neutral pH. It is +11 for pcDHFR, 0 for hDHFR, and –4 for ecDHFR. These differences could affect the electrostatic potential gradient at the active site (5). Thus, understanding the mechanism of catalysis and kinetics of substrate cofactor binding is important to the design of pcDHFR selective antifolates.

Analysis of a series of ecDHFR substrate–cofactor complex crystal structures has shown loop and subdomain movements in the enzyme conformation that led to a model for the molecular mechanism of DHFR catalysis, as well as to models for the transition-state geometry during catalysis (6–10). Comparison of ecDHFR NADP⁺, folate–NADP⁺, and apoenzyme complexes revealed disorder in the binding of the nicotinamide in the holoenzyme with concomitant

† Supported in part by Grant GM-51670 (V.C.) and NIH Contract NO1-AI-35171 (S.F.Q.).

‡ Protein Data Bank file name 1cd2.

* Corresponding author. E-mail: cody@hwi.buffalo.edu. Fax: (716) 852-6086.

§ Hauptman-Woodward Medical Research Institute, Inc.

|| Indiana University School of Medicine.

¹ Abbreviations: pcDHFR, *P. carinii* dihydrofolate reductase; FA, folic acid; MTX, methotrexate; ec, *E. coli*; NADPH, nicotinamide diphosphate adenine ribose.

mobility in the Met-20 loop (residues 16–20) involved in binding the nicotinamide ring of NADP⁺. These data suggested a model for the binding of 7,8-dihydrofolate in the Michaelis complex and for the transition-state complex (6, 8), as well as a mechanism for cooperativity in binding between substrate and coenzyme (6, 7). Further analysis of this series of ecDHFR structures showed subdomain rotation and mobility of the *p*-aminobenzoylglutamate cleft with substrate binding that is important for catalysis (10).

To date, no similar loop and subdomain movements have been observed in eukaryotic DHFR structures. For the first time, current studies of pcDHFR complexes with folate and NADP⁺ reveal structural evidence for ligand-induced conformational changes in nonbacterial DHFR. These data for pcDHFR indicate a mechanism for subdomain rotation and loop folding for release of NADP⁺ similar to that found in ecDHFR.

To investigate the structural basis for the mechanism of pcDHFR catalysis, we focused on the folate binary and folate–NADP⁺ ternary complexes with pcDHFR and compared the latter with the binding of methotrexate and NADPH. We report the crystal structures of the pcDHFR binary complex with folate, two ternary complexes with folate and NADP⁺, and a ternary complex with methotrexate and NADPH.

EXPERIMENTAL PROCEDURES

Crystallization and X-ray Data Collection. Recombinant pcDHFR was cloned, isolated, and purified as previously described (11). Although the enzyme preparation contained no protein contaminants, the sample was yellow in color. As noted previously (4), DHFR samples can contain a folate-like substance that is tightly bound to the enzyme and can be removed only with extensive isoelectric focusing or chromatofocusing chromatography. Although these samples were washed several times with buffer in the presence of NADPH, the ratio of absorbance at 280 nm to that at 320 nm was not greater than 20. The structure solution later revealed residual folate binding in these pcDHFR crystals. Incubation of these samples prior to crystallization revealed that hydrophobic, more weakly bound inhibitors were not able to displace the endogenous folate, whereas tight binding inhibitors were able to displace the residual folate from the same preparation of pcDHFR.

Prior to crystallization screens, the protein was washed in a centricon-10 concentrator three times with 50 mM MES buffer at pH 6.0 in 100 mM KCl buffer and concentrated to 14.3 mg/mL. A novel thermal gradient technique was used to carry out the crystallization screens with pcDHFR. For this method, we used micropipet or 0.7 mm X-ray capillary tubes for crystallization. The solubilized protein is first placed in an Eppendorf microcentrifuge tube in which the crystallizing buffer, and any additives, have been added. The tube contents are centrifuged at high speed to mix and pull the solution to the bottom of the tube. Capillary action is used to fill the micropipet or capillary which is then sealed using either heat, high-vacuum grease, or Cha-Seal clay. The batch experiments were positioned on the thermal gradient screening between 8.6 and 30.0 °C and allowed to equilibrate (12, 13, 26).

Crystallization of what turned out to be the pcDHFR–folate (FA) binary complex was carried out by adding 10 μ L of protein, 3 μ L of MES/KCl buffer, and 7 μ L of 50% (w/v) PEG 2000 in 50 mM MES (pH 6.0) and 100 mM KCl and placing the mixture in 0.7 mm X-ray capillaries for equilibration on a thermal gradient device. Samples of pcDHFR were also incubated with NADP⁺ along with different hydrophobic pcDHFR inhibitors and incubated overnight at 4 °C. The protein was washed to remove excess inhibitor and cofactor and concentrated to 9.8 mg/mL. These samples were set up with 40% (w/v) PEG 2000 with 50 mM MES and 100 μ M KCl buffer (pH 6.0) and placed on the thermal gradient device. Crystals grew primarily in the mid range of the temperature gradient.

Data collection was carried out at room temperature on the best crystals available for all samples to 2.0 Å resolution using a Rigaku RaxisIIc Imaging plate system with a rotating anode source. Diffraction data showed the presence of two crystal forms for the folate complexes: a monoclinic lattice for the ternary complexes and an orthorhombic lattice for the binary complex as illustrated in Table 1. Crystals of the MTX complex are also monoclinic. This is the first report of a pcDHFR complex in an orthorhombic space group, as previous pcDHFR complexes have been reported only in the monoclinic space group, *P*₂₁ (14–17).

Structure Determination and Refinement. The structures of all pcDHFR complexes were solved by molecular replacement methods with the program X-PLOR (18) used to orient the enzyme in the *P*₂₁2₁2₁ lattice based on the coordinates of the pcDHFR from the MTX ternary structure (16). Refinement was continued using the restrained least-squares program PROLSQ (19, 27) (modified by G. D. Smith, Hauptman-Woodward Medical Research Institute, Inc.) in combination with the model-building program CHAIN (20). All calculations were carried out on a Silicon Graphics Impact R1000 workstation. The initial $(2|F_o| - |F_c|) \exp i\alpha_c$ maps, where F_o is the observed and F_c the calculated structure factors, respectively, based on the protein model only and α_c is the calculated phase, resulted in electron density corresponding to both the inhibitor MTX, substrate FA, and the cofactor, NADPH or NADP⁺, as well as a good fit of the protein to its density. In the case of the FA binary structure, the flexible regions near encompassing loops 23 and 47 were rebuilt on the basis of omit maps from refinements in X-PLOR using simulated annealing protocols.

Further restrained refinement was continued for the ternary complexes, including the cofactor and inhibitor. The aromatic rings of folate and NADPH were constrained to be planar. Between least-squares minimizations, the structures were manually adjusted to fit the difference electron density and verified by a series of omit maps calculated from the current model with deleted fragments. Electron densities for residues 1–4 of the binary FA pcDHFR complex could not be interpreted, and no coordinates for these residues are reported.

The final refinement statistics are summarized in Table 1. The Ramachandran conformational parameters from the last cycle of refinement for all structures generated by PROCHECK (21) show that all structures have acceptable conformations as defined by PROCHECK criteria based on statistics from the Protein Data Bank. The range of most

Table 1: Crystal Properties and Refinement Statistics for pcDHFR Complexes

	MTX–NADPH	FA–NADP ⁺ (1)	FA–NADP ⁺ (2)	FA
lattice (Å)	37.425, 43.556, 61.659 $\beta = 94.89$	37.506, 43.115, 61.255 $\beta = 94.77$	37.305, 43.145, 61.141 $\beta = 94.77$	38.048, 61.510, 85.665
space group	$P2_1$	$P2_1$	$P2_1$	$P2_12_12_1$
resolution range (Å)	8.0–2.5	8.0–1.9	8.0–2.2	8.0–2.0
no. of reflections used (2σ)	5821	12871	8596	11837
R factor (%)	17.3	20.0	19.8	19.5
no. of protein and heteroatoms	1728	1761	1761	1762
no. of water molecules	48	51	77	55
B factor (protein average) (Å ²)	18.99	28.41	23.78	22.28

target σ	root-mean-square deviation			
distances (Å)	monoclinic	monoclinic (1)	monoclinic (2)	orthorhombic
bonds (0.020)	0.014	0.020	0.015	0.019
angles (0.040)	0.047	0.053	0.048	0.048
planar 1–4 (0.050)	0.049	0.056	0.050	0.051
nonbonded distances				
single torsion (0.500)	0.207	0.205	0.211	0.208
planar groups (0.02)	0.012	0.015	0.014	0.015
chiral volume (0.15)	0.160	0.215	0.192	0.192
multiple torsion (0.50)	0.263	0.277	0.280	0.258
hydrogen bonds (0.50)	0.246	0.281	0.290	0.220
torsion angles (deg)				
planar (3.0)	2.2	2.5	2.1	2.4
tagged (15.0)	21.1	21.1	22.5	19.9
orthonormal (20.0)	24.9	20.3	25.4	19.5

avored conformations for all structures was between 86 and 90%. Coordinates for these structures have been deposited with the Protein Data Bank (file name 1cd2).

RESULTS

Overall Structure. The structures of the three pcDHFR FA complexes are compared with that of pcDHFR–MTX–NADPH (Figure 1). The two FA NADP⁺ ternary structures are similar to each other with the exception of the backbone conformation between residues 83 and 90, and are more similar to the MTX complex than to the folate binary complex of pcDHFR which has regions that differ significantly in backbone conformation.

The major conformational differences between the pcDHFR FA binary complex and the others are movement of loop 23 (residues 19–29) which has a maximum displacement of 7.3 Å from the folate NADP⁺ ternary complexes, and 6.7 Å from the MTX NADPH complex with pcDHFR (Figure 2), and loop 47 (residues 45–50) (Figure 1). These data further show that the region between residues 151 and 154 within the F–G loop of pcDHFR moves in concert with the conformation of loop 23. As highlighted in Figure 2, there are three distinct positions for loop 23 among these structures with the binary FA structure having a new “flap-open” conformation and a “closed” conformation over the nicotinamide–ribose of the cofactor in the three ternary complexes.

On the basis of the analysis of more than 40 ecDHFR crystal structures, three distinct conformational states have been identified for the flexible Met-20 loop (residues 10–24): open, closed, and occluded, which are characterized by their secondary structure, interactions with NADPH, and hydrogen bonding patterns (10). The mechanism of the flexible loop movement in ecDHFR has been considered a

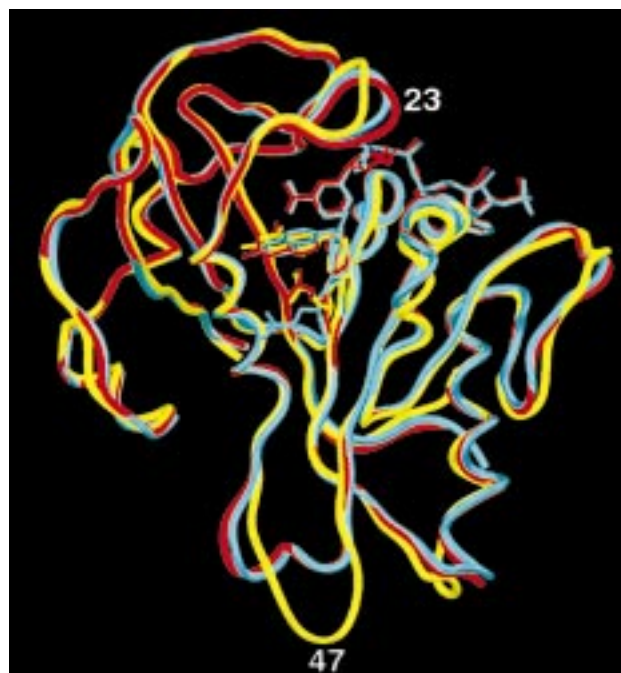


FIGURE 1: Ternary structures of pcDHFR complexes illustrating ligand-induced conformational differences in the binding substrate, inhibitor, and cofactor. α -Carbon trace of pcDHFR for the FA binary complex (yellow), for the FA–NADP⁺ ternary complex (cyan), and for the MTX–NADPH ternary complex (red). The largest conformational differences are noted near loops 23 and 47. Note the movement of loop 23 in a “flap-open” and “closed” position over the nicotinamide–ribose of the cofactor. Also note the unwinding of the short helical turn at loop 47. The figure was made with the program SETOR (24).

thermodynamic equilibrium between the “closed” and “occluded” conformation that blocks cofactor binding and shifts in favor of the “closed” conformation by binding of the



FIGURE 2: Stereo comparison of loop 23 (Gly-20-Arg-21-Ser-22-Asn-23-Ser-24-Leu-25-Pro-26-Trp-27) conformations in the pcDHFR FA binary complex (thick line), the two FA NADP⁺ ternary complexes (thin lines), and the MTX NADPH ternary complex (dashed line).

nicotinamide—ribose of NADPH, and with stabilization of the loop conformation by van der Waals contacts. This binding is further stabilized by interactions with the substrate. These data show that the closed and occluded conformations occupy the extremes of movement with intermediate characteristics for the open conformation (10).

In the pcDHFR structures reported here, a similar “closed” loop conformation (residues 19–29) is observed in the three ternary pcDHFR complexes, similar to that characterized for ecDHFR (10). This loop conformation is stabilized by a series of hydrogen bonds between Arg-21, Ser-22, and Ser-24, and the O2 hydroxyl of the nicotinamide—ribose which forms a hydrogen bond contact with the backbone N of Ser-24. Additionally, in the FA NADP⁺ ternary pcDHFR complexes, the carbonyl of Arg-21 interacts with a structural water that is not observed in the MTX NADPH pcDHFR ternary complex. Similar to the “closed” loop conformation in ecDHFR, hydrogen bond interactions with Gly-20, Ser-22, and Asp-153 of the F–G loop are also maintained.

The main characteristic of the open loop conformation in ecDHFR is a shift in the positions of residues 18 and 19 away from the nicotinamide—ribose ring, thus opening the cofactor binding pocket. However, there is no evidence for such a shift in these pcDHFR ternary complexes. Since the backbone conformation of loop 23 for MTX–NADPH pcDHFR is similar to those of the FA–NADP⁺ pcDHFR complexes (Figure 1), the primary difference between these loop structures is translational and does not reflect an open loop conformation.

The occluded conformation described for the ecDHFR complexes blocks the nicotinamide binding pocket by a 180° rotation about Ψ of residue Ile-14 that also disrupts hydrogen bonding with the F–G loop of ecDHFR (10). There is no evidence of such a conformation in these pcDHFR complexes. In fact, the conformation for loop 23 in the binary FA pcDHFR complex represents a distinctly new “flap-open” conformation that has not been observed for any of the ecDHFR complexes and is characterized by a >7 Å shift away from the closed position. Despite the large conformational change in loop 23 for the binary complex, hydrogen bond contacts with the F–G loop through residue Asp-153 are maintained and highlight the concerted nature of these interactions.

Another major conformational change occurs at loop 47 (residues 45–50) of the FA binary structure (Figure 1). This is the first observation of such a large conformational change in the DHFR tertiary structure. Alignment of the sequences for pc- and ecDHFR reveals that there is no corresponding loop in the bacterial structure as pcDHFR has a 17-residue insertion compared to the bacterial DHFR sequence. In the MTX and FA ternary pcDHFR complexes, this region forms a short helical turn which has unwound in the binary FA pcDHFR complex. The unexpected consequence of this change is exposure of Phe-46 and Phe-49 to the enzyme surface, and placing Asp-48 away from the surface, as compared to their conformations in the other ternary pcDHFR complexes. This change also results in a redistribution of the surface charges as illustrated in the electrostatic potential representation in Figure 3. The electron density in this region of the binary complex is well-defined, and thermal parameters for this region are similar to those in adjacent secondary elements, validating the stability of this feature.

Ligand or Inhibitor Binding. In the case of the three oxidized cofactor structures, no exogenous folate was added to the crystallization media, although in the two monoclinic crystals, incubation with hydrophobic inhibitors was carried out. Therefore, the density for a folate-like molecule was unexpected. As illustrated (Figure 4), there was no ambiguity in the interpretation of this density as fitting a molecule of folate, unlike that observed for the naphthyl—furopyrimidine pcDHFR complex (17). However, much higher resolution data are needed to precisely identify any stereochemical modifications to the ligand. Therefore, this density is assumed to be a folate-like structure.

Although no protein contamination was indicated by polyacrylamide gel electrophoresis, the pcDHFR enzyme samples had a yellowish color and an absorbance atypical for a protein without chromophores. These phenomena have been observed by others, and it has been surmised that this contaminant is most likely a degradation product of dihydrofolate that is tightly bound to the enzyme (4). Furthermore, it is likely this contaminant represents a small proportion of the total sample. However, upon crystallization in the presence of weakly binding inhibitors, such as the more hydrophobic analogues studied here, the complex with the contaminant is apparently more stable and predominates nucleation.

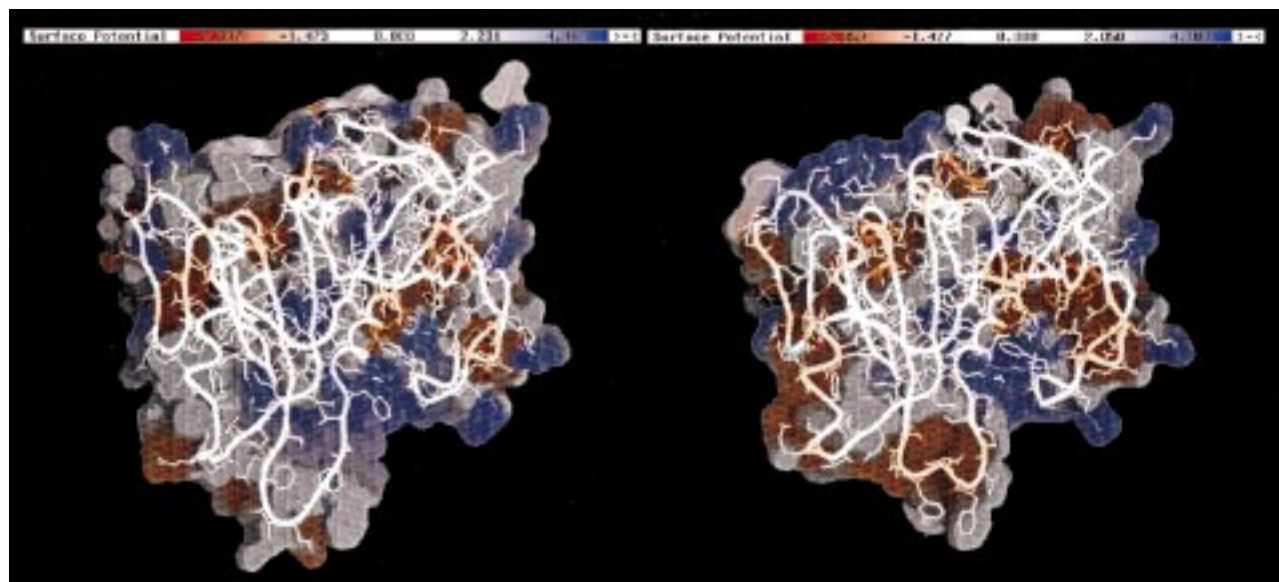


FIGURE 3: GRASP electrostatic potential surface for the pcDHFR–FA binary complex (left) and the pcDHFR–FA–NADP⁺ ternary complex (right) highlighting the effect of conformational changes in loop 47 on the electrostatic potential surface (25). White is neutral, blue positive, and red negative.



FIGURE 4: Stereoview of the fit of folate to the difference electron density ($F_o - F_c$, 3σ) calculated from an omit map from the XPLOR refinement.

The binding orientation of the pteridine ring of FA in these structures is similar to that observed in hDHFR FA binary complexes (22, 23). The overall pattern of ligand interactions with the acidic function in the DHFR active site is preserved as shown by the hydrogen bonds of the conserved residues (Thr-144 and Trp-27, and structural waters) (Figure 5). The major change that results from the reorientation of the pteridine ring of folate and methotrexate involves the shift in hydrogen bonding partners with Glu-32. In the folate complexes, the carboxylate oxygens OE2 and OE1 of Glu-32 interact with N(3) and the 2-amino group, whereas in MTX, the carboxylate oxygens interact with the 2-amino group and N(1) (Figure 5). In addition, the carboxylate oxygens of the glutamate in both complexes form hydrogen bonds with a conserved Thr-144 and with a conserved Trp-27, as well as with the conserved structural waters (14, 15). In these FA–NADP⁺ pcDHFR structures, there is no evidence of a structural water molecule near N5 of the folate molecule whose presence was postulated to play a role in catalysis for the bacterial DHFR enzyme (9, 10). However, there is a structural water molecule mediating a hydrogen bond network between the N10 of the folate, the O1 of the

nicotinamide ribose, and Ser-64 in the folate NADP⁺ ternary pcDHFR complexes. The interactions with water have been suggested to help stabilize a transition-state geometry between the substrate and cofactor (9).

A further consequence of the reorientation of the pteridine ring is the loss of hydrogen bond interactions involving the 4-amino group (Figure 5) with conserved residues Ile-10, Leu-123, and Tyr-129. There are no hydrogen bonds with these residues formed by FA. In addition, in the FA ternary pcDHFR complexes, the 4-O hydrogen bonds with the structural water that is part of the hydrogen bonding network involving Glu-32 and Trp-27 (Figure 5). In the MTX pcDHFR complex, this structural water interacts with the pteridine N8.

NADP⁺ Binding. Although NADP⁺ is bound in an extended conformation, similar to other cofactor complexes (14, 15), there is variation in the conformation of the nicotinamide–ribose and the pyrophosphate moieties (i.e., θ_n and ψ_n ; Table 2). The conformations of the nicotinamide–ribose moiety in the two FA complexes are similar to that observed for NADPH in the MTX complex with the exception of the C9–C10–O4–Pn bond which is trans in

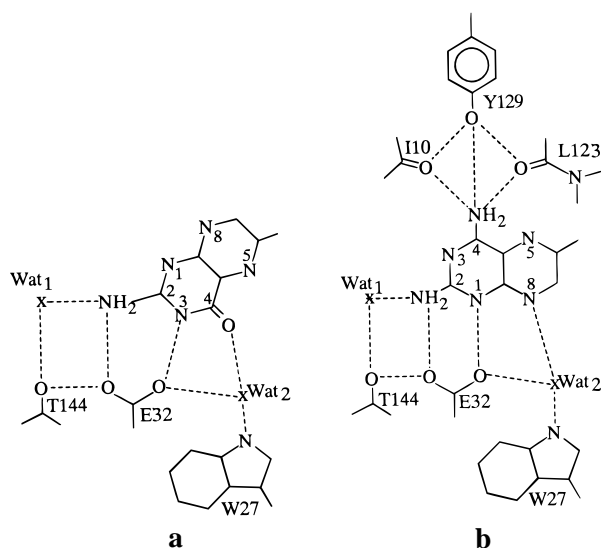
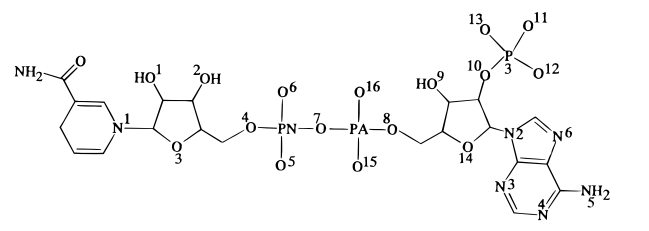


FIGURE 5: Hydrogen bond geometry involving the pteridine ring for (a) folate and (b) MTX in the pcDHFR active site. This network of hydrogen bond interactions with two structural waters and invariant residues Thr-144, Glu-32, and Trp-27 are characteristic of all folate complexes reported to date. In addition to preserving the hydrogen bond network observed for the folates, the 4-amino group of MTX interacts with invariant residues Ile-10, Tyr-129, and Leu-125.

Table 2: Cofactor Conformation in pcDHFR Ternary Complexes with FA and MTX^a



NADPH or NADP ⁺	torsion angle	MTX in P ₂₁	FA (1) in P ₂₁	FA (2) in P ₂₁
χ_n	C5–N1–C6–C7	128.2	119.3	114.9
ξ_n	C8–C9–C10–O4	–168.3	–178.4	–167.5
θ_n	C9–C10–O4–P _n	165.7	123.7	127.3
ψ_n	C10–O4–P _n –O7	59.3	67.3	64.0
φ_n	O4–P _n –O7–P _a	105.9	58.9	39.7
φ_a	P _n –O7–P _a –O8	118.6	176.4	–170.1
ψ_a	O7–P _a –O8–C11	–77.6	–61.5	–55.5
θ_a	P _a –O8–C11–C12	–152.8	–149.5	–155.2
ξ_a	O8–C11–C12–C13	–170.9	164.6	167.3
χ_a	C14–C15–N2–C20	–122.7	–114.8	–116.9
θ'_a	C15–C14–O10–P2	163.4	162.8	164.6

^a Subscript n denotes torsion angles for nicotinamide nucleoside; subscript a denotes torsion angles for adenine nucleoside. Values are in degrees.

the MTX ternary pcDHFR complex, and is +gauche in the folate complexes (Table 2). The geometry about the pyrophosphate bridge shows the greatest variation. Also, torsion angle φ_a is +gauche for MTX and trans for the FA binary complex (Table 2). Furthermore, differences in the loop 23 conformation for the MTX–NADPH ternary pcDHFR complex are related to differences in the nicotinamide–ribose conformation and that observed for the FA–NADP⁺ ternary complexes. These changes place the MTX loop 23 between the extremes observed for the folate structures (Figure 2).

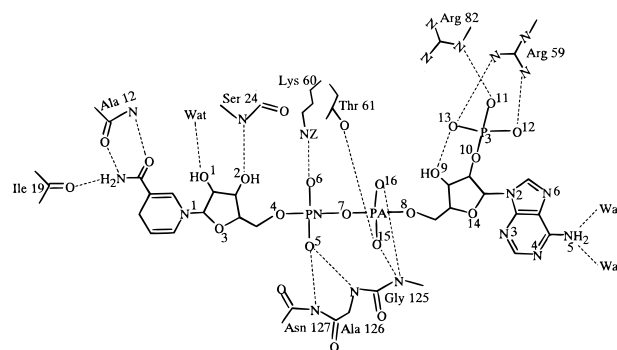


FIGURE 6: Schematic representation of the pcDHFR interactions with the cofactor NADP⁺. Note that the cis conformation for Gly-124 and Gly-125 permits the N of Gly-125 to insert itself between the pyrophosphate oxygens (O15 and O16). This feature is conserved in all DHFR structures.

The carboxamide group of the nicotinamide ring, which is syn to the nicotinamide ring N, makes a series of strong hydrogen bonds with conserved residues Ala-12 and Ile-19 in pcDHFR. In addition, there are a series of nonbonded C–H···O contacts involving the nicotinamide ring carbons and three neighboring oxygens of residues Leu-9, Ile-19, and Leu-123 which lie approximately in the plane of the nicotinamide ring. These features are conserved in ternary complexes from most species of DHFR (8, 14, 15).

Illustrated in Figure 6 are the enzyme contacts with the cofactor, NADP⁺ or NADPH. There is a cis peptide linkage between Arg-67 and Pro-68 and Gly-124 and Gly-125, as observed in other pcDHFR complexes (14, 15). The cis conformation of the invariant glycines permits interaction with the pyrophosphate oxygens that are positioned at the end of central helix C. The largest change involves the ribose conformation of the nicotinamide–ribose ring (Table 2). In the folate pcDHFR complexes, the ribose O1 hydroxyl interacts with a structural water, not present in the MTX complex because of the N10-methyl substituent, and the ribose O2 hydroxyl interacts with the hydroxyl of Ser-64 of the closed loop. The overall interactions for the cofactor with pcDHFR in the ternary complexes are similar. Hydrogen bond contacts with NADPH are tighter in the MTX NADPH ternary complex.

In the folate binary complex, the side chain of residues Arg-82, Lys-96, and Asn-127 changes conformation to fill the space occupied by the phosphate of the adenosine–ribose of FA NADP⁺ pcDHFR ternary complexes.

Packing Interactions. The unwinding of the short helical turn involving residues 45–50 of the pcDHFR ternary inhibitor or substrate complexes, placing the hydrophobic residues (Phe-46 and Phe-49) toward the protein surface, is stabilized by packing interactions present in the orthorhombic lattice for the binary FA pcDHFR complex. As illustrated (Figure 7), in this packing arrangement, Lys-73 from a symmetry-related enzyme forms a series of tight hydrogen bonds with the backbone carbonyl oxygens of both Phe-46 and Phe-49 (Table 3). In this conformation, the phenyl rings of residues 46 and 49 interact with the methylene carbons of residues Glu-63 and Ser-24 whereas Asp-47 hydrogen bonds to a water, and Glu-50 forms a series of hydrogen bond interactions with the backbone atoms of Ser-114 and Asn-116.

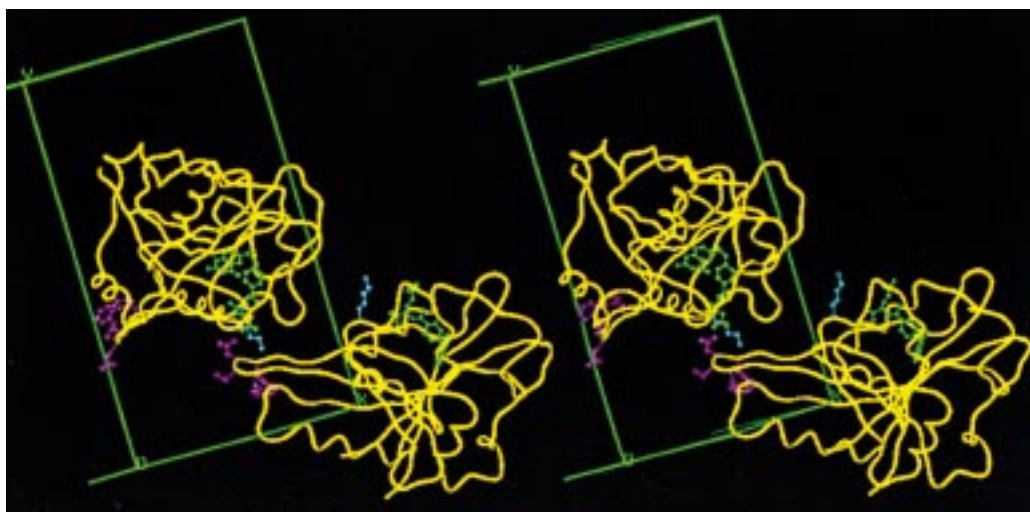


FIGURE 7: Stereodigram of the packing interactions involving loop 47 for the binary FA (green) pcDHFR complex in space group $P2_12_12_1$. Note that in this case, the amine from Lys-73 (cyan) of a symmetry-related molecule inserts itself in a pocket made by the unwound helical turn between residues 46 and 49 (violet). The Lys-73 amine forms close contacts with the backbone carbonyl oxygens of Phe-46 and Phe-49, as well as a contact with Glu-50. This stabilization results from the unwinding of the helical turn usually observed in this region in the monoclinic lattice.

Table 3: Hydrogen Bond Interactions of Loop 47 in pcDHFR

Monoclinic Lattice with Loop 47 in a Short Helical Turn Conformation	
Phe-46 O...N Ser-48	Phe-49 N...N Ser-48
Ser-48 Og...O Pro-44	Glu-50 OE1...Nz Lys-31 ^a
Orthorhombic Lattice with Loop 47 in an Extended Conformation	
Phe-46 O...Nz Lys-73 ^a	Ser-48 Og...NH1 Arg-70 ^a
Phe-49 O...Nz Lys-73 ^a	Asp-47 OD1...N Gln-67 ^a
Glu-50 OE2...Nz Lys-73 ^a	Asp-47 OD2...Wat

^a Refers to a symmetry-related molecule in the crystal lattice.

In the monoclinic lattice for the ternary pcDHFR complexes (Figure 8), the backbone N of Phe-46 forms intramolecular contacts with the backbone carbonyl of Pro-44, the N of Ser-48, and the carbonyl of Phe-49. Asp-47 interacts with the backbone N of Phe-49 and Glu-50 which in turn makes intermolecular contacts with the amino group of Lys-31 of a symmetry-related molecule (Table 3). The contacts are stronger for the MTX NADPH ternary pcDHFR complex and weaker for the FA ternary complexes. The phenyl rings of residues 46 and 49 interact with hydrophobic surfaces provided by Tyr-35, Phe-199, and Pro-186 of a symmetry-related molecule (Figure 8).

DISCUSSION

These crystallographic studies describe structural comparisons among four pcDHFR complexes and show the first example of ligand-induced conformational changes in pcDHFR with large movements of the flexible loops encompassing residues 19–26 (loop 23) and residues 45–50 (loop 47) in the folate binary pcDHFR complex compared to those of the ternary complexes. Although there is a pattern of flexible loop movement from open, closed, and occluded conformations in the bacterial structures, no open or occluded conformations have been observed in these pcDHFR structures, or for human DHFR complexes. The >7 Å shift in loop 23 from the new “flap-open” to the “closed” conformation on cofactor binding in pcDHFR has not been observed for any of the bacterial enzyme complexes, although the

“closed” conformations of the pcDHFR ternary complexes are similar to those observed for many ecDHFR structures.

Since little variation in the loop conformation was observed within a series of isomorphous ecDHFR structures, regardless of ligated state (10), it was suggested that crystal lattice contacts at one or more of the flexible loop regions (M20, F–G, or G–H loops) shifted the equilibrium in favor of a particular conformation. However, in the case of the orthorhombic lattice for the FA binary pcDHFR complex, there are no crystal contacts that cause the conformational changes observed in loop 23, whereas the unwinding of the short helical turn in loop 47 of the binary folate pcDHFR complex is clearly influenced by intermolecular packing interactions that stabilize this unexpected conformation. Such interactions are not possible in ecDHFR as the 17-residue deletion in the sequence removes this loop from the ecDHFR structure.

As a result of the conformational flexibility observed among these pcDHFR structures, subdomain movements can be assessed. In the case of the ecDHFR complexes, the enzyme was defined as having two subdomain structures: a flexible loop and an adenosine binding subdomain that show rotational and hinge movements between the subdomains (8–10). Similarly for pcDHFR structures, there is a shift in the helical regions that are involved with the pyrophosphate of the cofactor. As illustrated (Figure 9), helices B and F show little movement among these binary and ternary pcDHFR complexes, whereas helix C shows larger shifts. There is a maximum shift of 1.1 Å in helix C at residue Ile-65 between the folate binary and folate NADP⁺ ternary complex upon cofactor binding. This distance is slightly larger at Ser-64 (1.2 Å). The shift in helix C by the MTX NADPH ternary complex permits tighter hydrogen bonding interactions with the pyrophosphate oxygens (Figure 9, O16...Thr-61N). There is a 0.78 Å movement between the Thr-61 N atoms in the FA NADP⁺ and MTX NADPH structures. Further shifts are encountered in the position of FA and MTX in the *p*-aminobenzoyl cleft. For example, in these structures there is 1.3 Å shift of MTX out of the cleft compared to FA in the binary complex, but only 1.1 Å in the FA NADP⁺ ternary

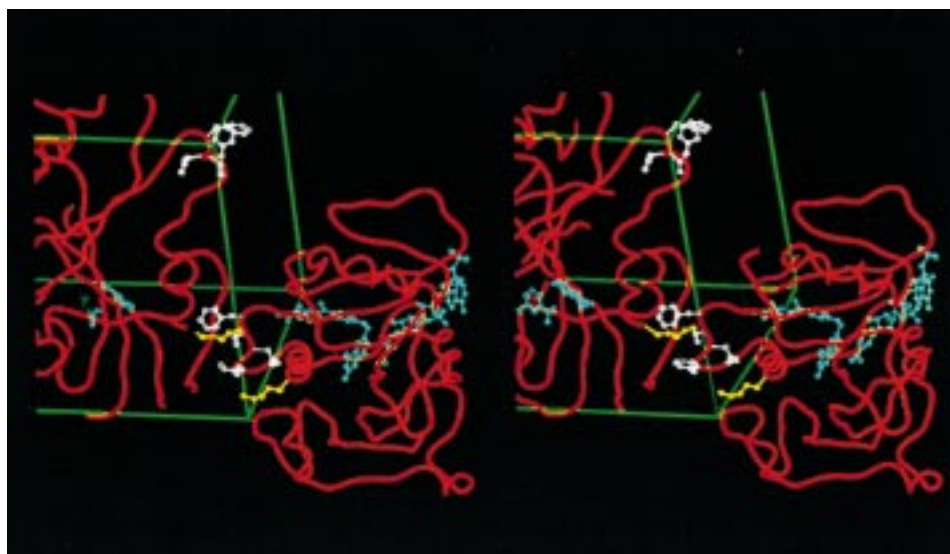


FIGURE 8: Stereodiagram of the packing interactions involving loop 47 (white) for the ternary FA NADP⁺ (cyan) pcDHFR complex in space group $P2_1$. Note that in this case, the amine from Lys-31 (yellow) of a symmetry-related molecule interacts with Glu-50. Phe-49 forms hydrophobic interactions with Tyr-35, Phe-199, and Pro-186 of a symmetry-related molecule, while Phe-46 makes hydrophobic contacts with the side chain methylenes of Gln-68 and Lys-31 of a symmetry-related molecule. These interactions are stabilized by the helical turn of this loop.

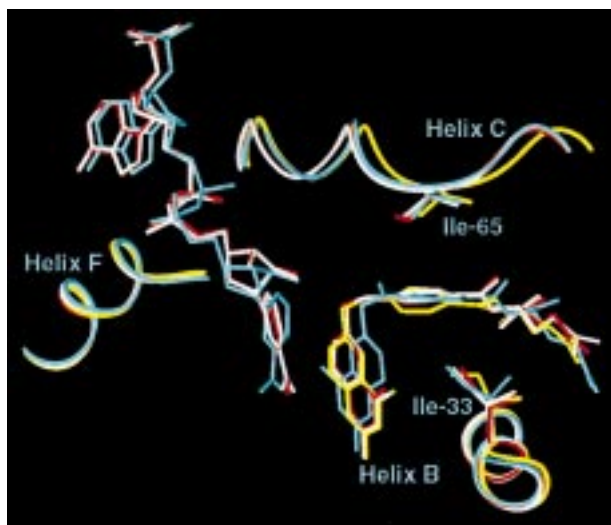


FIGURE 9: Comparison of the helices surrounding the cofactor and substrate in pcDHFR complexes (yellow, FA; white and red, FA NADP⁺; and cyan, MTX NADPH). As illustrated, there is little movement in the positions of helices B and F, while the position of helix C is more variable, as observed in the ecDHFR structures (10). Also highlighted are hydrophobic active site residues Ile-33 and Ile-65.

complex. These distances become more divergent near the cleft entrance when there is 2.7 Å difference in the g-COOH oxygen of FA in the ternary complex (1.37 Å for FA and MTX) due to conformational changes in the carboxylate hydrogen bonding interactions.

Comparison of the ternary complexes for FA–NADP⁺ and MTX–NADPH (Figure 10) reveals a possible transition-state geometry for the transfer of a hydride to C6 of FA. In contrast, the reorientation of MTX in the active site compared to that of FA shows a nonproductive enzyme state and thus inhibition of the enzyme mechanism. Bystroff and Kraut (7) proposed a hypothetical model of the conformational changes that may be involved in the transition state of ecDHFR. Key elements of this model were the shift in the position of helix

C producing tighter binding to the pyrophosphate of NADPH which is anchored to a more rigid helix F. These data suggested that the side chain of the active site Leu-28 in ecDHFR makes short contacts with substrate positions C6 and C15 during the transition state. In the pcDHFR complexes (Figure 9), these geometries are apparently not as strained, since there are no unusually close contacts between Ile-33 and these atoms in FA.

In the ecDHFR structure, the van der Waals surfaces for residues Ile-50 and Leu-28 overlap, indicating a more compact environment for the bacterial enzyme (10). However, in the pcDHFR structures the contacts of hydrophobic residues Ile-65 and Ile-33 with the benzoyl ring of FA or MTX are not as compact and may explain the weaker binding affinity of FA and MTX for pcDHFR than for ecDHFR (Figure 9). There is a significant rotation of the benzoyl ring in MTX compared to those of the FAs. These changes place the ring of MTX closer to that of Ile-33 and to Ile-65 in these structures (3.4 vs 4.3 Å and 3.8 vs 4.3 Å for residues 33 and 65, respectively).

Kinetic data for pcDHFR show that in many aspects, the pc enzyme shares enzymatic properties with both bacterial and human enzymes. However, unlike the bacterial and human enzymes, there is only one preferred pathway for catalytic function (4). On the basis of the structural data for the apo, holo, binary, and ternary ecDHFR, a model correlating the conformational changes with the multiple pathways in the catalytic cycle was proposed that revealed the role of the flexible Met-20 loop of ecDHFR in the catalytic cycle. Unlike those for ec- and hDHFR, kinetic data for pcDHFR point to a single, preferred pathway with a rapid dissociation of NADP from the ternary product complex. Furthermore, the dissociation of tetrahydrofolate from its binary complex is slower than that of the human enzyme with negligible formation of the apoenzyme at any time (4, 5). Structural data for these pcDHFR complexes indicate that the role of the flexible loop 23 is similar to that defined in the ecDHFR catalytic cycle. Moreover, the larger, “flap-

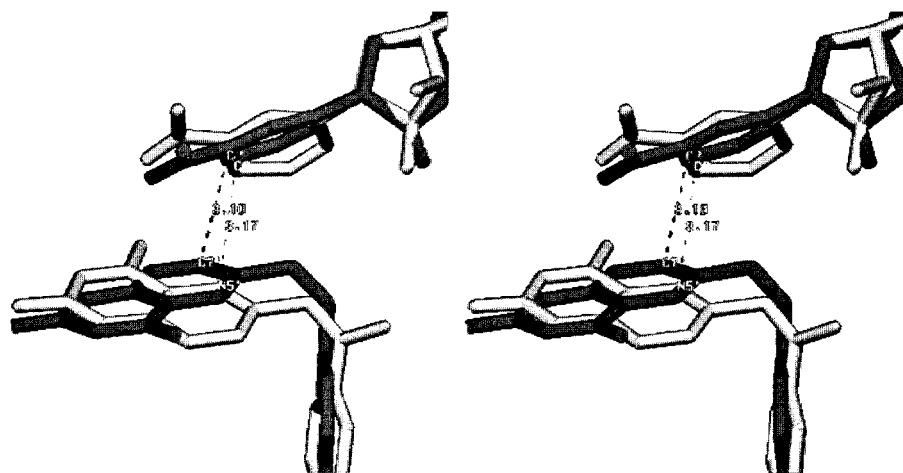


FIGURE 10: Comparison of the conformation between folate and NADP⁺ (light) and the MTX and NADPH inhibitor complex (dark). Note the closest contacts between the C7 of FA and the C2 of the nicotinamide ring (3.10 Å) and the N5 of MTX and C2 of the nicotinamide (3.17 Å) are similar, suggesting that these represent nonproductive transition-state geometries.

open” conformation observed for the binary FA complex is consistent with the rapid release of cofactor as the binding cavity is more open. Even in the “closed” position, the contacts with cofactor and substrate are weaker than those observed for the bacterial enzyme and are conducive for the rapid dissociation of substrate product from the ternary complex. Also, the failure to observe an occluded conformation for the binary FA complex is consistent with kinetic data showing negligible formation of an apoenzyme state.

To date there has been no observation of similar flexible loop formation in the human DHFR structures. However, there are not sufficient data to indicate whether this is due to the stability of the hDHFR structure or due to the lack of appropriate crystallization conditions for stabilizing such conformations. It would be expected that hDHFR experiences conformational states similar to those of ecDHFR since it also has multistep catalytic pathways (4, 5).

Overall, these structural results reveal a novel “flap-open” loop 23 conformation for the FA binary complex with pcDHFR, as well as the “closed” loop 23 conformation that was postulated to play a role in the catalytic cycle of ecDHFR. The analysis of the movements of secondary elements that make up the subdomains as defined for ecDHFR (8–10) reveals a similar pattern in that movement of helix C in the binary complex and correlates well with the catalytic pathway defined for pcDHFR.

On the basis of these data, a model could be proposed for the apo pcDHFR structure that is similar to the “flap-open” conformation rather than the occluded conformation of ecDHFR as this would require fewer conformational changes to afford cofactor and ligand binding which is consistent with the rapid dissociation of the cofactor from the product complex. The weaker contacts in the “closed” conformation of pcDHFR compared to those of the bacterial enzyme are also consistent with faster substrate release. Therefore, these structural observations are supportive of the single, preferred reaction path defined for pcDHFR catalysis.

ACKNOWLEDGMENT

V.C. thanks G. Dave Smith for use of his protein analysis programs and for his helpful discussions with the X-PLOR programs, and Ray Blakley for his helpful discussions.

REFERENCES

1. Mills, J. (1986) *Rev. Infect. Dis.* 8, 1001–1011.
2. Kovacs, J. A., Hiemenz, J. W., Macher, A. M., Stover, D., Murray, H. W., Shelhamer, J., Lane, H. C., Urmacher, C., Honig, C., Longo, D. L., Parker, M. M., Natanson, C., Parrillo, J. E., Fauci, A. S., Pizzo, P. A., and Maur, H. (1984) *Ann. Intern. Med.* 100, 663–671.
3. Kovacs, J. A., and Maur, H. (1988) *J. Infect. Dis.* 158, 254–259.
4. Margosiak, S. A., Appleman, J. R., Santi, D. V., and Blakley, R. L. (1993) *Arch. Biochem. Biophys.* 305, 499–508.
5. Blakley, R. L. (1995) in *Advances in Enzymology and Related Areas of Molecular Biology* (Meister, A., Ed.) Vol. 70, pp 23–102, Wiley, New York.
6. Bystroff, C., Oatley, S. J., and Kraut, J. (1990) *Biochemistry* 29, 3263–3277.
7. Bystroff, C., and Kraut, J. (1991) *Biochemistry* 30, 2227–2239.
8. Brown, K. A., and Kraut, J. (1992) *Faraday Discuss.* 93, 217–224.
9. Reyes, V. M., Sawaya, M. R., Brown, K. A., and Kraut, J. (1995) *Biochemistry* 34, 2710–2723.
10. Sawaya, M. R., and Kraut, J. (1997) *Biochemistry* 36, 586–603.
11. Broughton, M. C., and Queener, S. F. (1991) *Antimicrob. Agents Chemother.* 35, 1348–1355.
12. DeTitta, G. T., Dembik, D. M., Pangborn, W. A., and Luft, J. R. (1996) *Acta Crystallogr.* A52, C504.
13. Luft, J. R., Rak, D. M., and DeTitta, G. T. (1999) *J. Crystal Growth* 196, 447–449.
14. Champness, J. N., Achari, A., Ballantine, S. P., Byrant, P. K., Delves, C. J., and Stammers, D. K. (1994) *Structure* 2, 915–924.
15. Cody, V., Galitsky, N., Luft, J. R., Pangborn, W., Gangjee, A., Devraj, R., Queener, S. F., and Blakley, R. L. (1997) *Acta Crystallogr.* D53, 638–649.
16. Cody, V., Galitsky, N., Luft, J. R., Pangborn, W., Gangjee, A., and Queener, S. F. (1997) in *Chemistry and Biology of Peridines and Folates* (Pfleiderer, W., and Rokos, H., Eds.) pp 399–402, Blackwell Science, Berlin.
17. Gangjee, A., Guo, X., Queener, S. F., Cody, V., Galitsky, N., Luft, J. R., and Pangborn, W. (1998) *J. Med. Chem.* 41, 1263–1271.
18. Brunger, A. T. (1992) *XPLOR*, Yale University Press, New Haven, CT.
19. Hendrickson, W. A., and Konnert J. H. (1980) in *Computing in Crystallography* (Diamond, R., Ramaseshan, S., and Venkatesan, K., Eds.) p 13.01, Indian Academy of Sciences, Bangalore, India.

20. Sack, J. S. (1988) *J. Mol. Graphics* 6, 224–225.
21. Laskowski, R. A., MacArthur, M. W., Moss, D. S., and Thornton, J. M. (1993) *J. Appl. Crystallogr.* 26, 283–291.
22. Oefner, C., D'Arcy, A., and Winkler, F. K. (1988) *Eur. J. Biochem.* 174, 377–385.
23. Davies, J. F., Delcamp, T. J., Prendergast, N. J., Ashford, V. A., Freisheim, J. H., and Kraut, J. (1990) *Biochemistry* 29, 9467–9479.
24. Evans, S. V. (1993) *J. Mol. Graphics* 11, 148–153.
25. Nicholls, A., and Honig, B. (1991) *GRASP*, Columbia University, New York.
26. Luft, J. R., Rak, D. M., and DeTitta, G. T. (1999) *J. Crystal Growth* 196, 450–455.
27. Finzel, B. C. (1987) *J. Appl. Crystallogr.* 20, 53.

BI982728M